Research Article | Open Access

Iontronics

Lou *et al. Iontronics* **2026**, *2*, 3 **DOI:**10.20517/iontronics.2026.03

Neurochemical memory diversification towards liquid reinforcement learning

Hao Lou[1,#], Cheng Yuan[1,#], Yuan-Cheng Zhu[2], Feng-Zao Chen[3], Hui-Min Jia[4], Jing-Juan Xu[1], Wei-Wei Zhao[1,3]

Keywords:
Neurochemical, memory diversification, reinforcement learning, liquid system, neuromorphic engineering

Citation: Lou, H.; Yuan, C.; Zhu, Y. C.; Chen, F. Z.; Jia, H. M.; Xu, J. J.; Zhao, W. W. Neurochemical memory diversification towards liquid reinforcement learning. *Iontronics* **2026**, *2*, 3. https://dx.doi.org/10.20517/iontronics.2026.03

Received: 27 Nov 2025
First Decision: 16 Dec 2025
Revised: 29 Dec 2025
Accepted: 31 Dec 2025
Published: 13 Jan 2026

Academic Editor:
Di Wei
Copy Editor:
Shu-Yuan Duan
Production Editor:
Shu-Yuan Duan

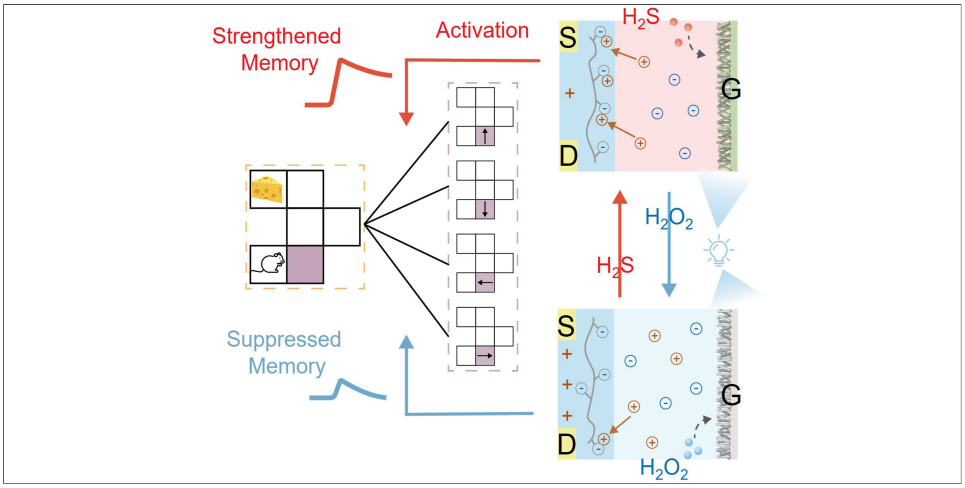

Abstract

The creation of biological memory analogs has long been hindered by the fundamental mechanistic differences between solid-state electronics and biological systems. By manipulating biomolecules in appropriate electrolytic environments, aqueous emulation of memory and its diversification has recently emerged. Here, we present real neurochemical memory diversification based on a nascent organic photoelectrochemical transistor and its implementation toward liquid reinforcement learning (RL). By employing neurochemicals H_2S and H_2O_2 as reward and clearance signals, respectively, the device demonstrates reversible switching between strengthened and suppressed memory, reproducing diversified memory behaviors analogous to those in the human brain. As its diversified memory supports adaptive decision-making and strategy updating, it is further applied to a navigation task for efficient RL. This work provides a strategy for aqueous neurochemical memory diversification and highlights liquid-phase RL for advanced neuromorphic applications.

[1]State Key Laboratory of Analytical Chemistry for Life Science, School of Chemistry and Chemical Engineering, Nanjing University, Nanjing 210023, Jiangsu, China.
[2]State Key Laboratory of Pharmaceutical Biotechnology, School of Life Sciences, Nanjing University, Nanjing 210023, Jiangsu, China.
[3]Zhejiang Key Laboratory of New Drug Development for Central Nervous System Diseases, School of Pharmaceutical and Chemical Engineering, Taizhou University, Taizhou 318000, Zhejiang, China.
[4]Key Laboratory of Micro-Nano Materials for Energy Storage and Conversion of Henan Province, Institute of Surface Micro and Nano Materials, Xuchang University, Xuchang 461000, Henan, China.
[#]These authors contributed equally to this work.

Correspondence to: Prof. Jing-Juan Xu, Prof. Wei-Wei Zhao, State Key Laboratory of Analytical Chemistry for Life Science, School of Chemistry and Chemical Engineering, Nanjing University, Nanjing 210023, Jiangsu, China. E-mail: xujj@nju.edu.cn; zww@nju.edu.cn

INTRODUCTION

Memory is one of the most important physiological functions of the human brain wherein information is encoded, stored and retrieved[1-3]. Inspired by this, artificial memory devices have been increasingly pursued in neuromorphic engineering toward advanced artificial intelligence and the Internet of Things[4-6]. As very recently summarized by Samorì *et al*., memory diversification has been actively pursued in various solid-state electronics via a plethora of optical, electrical, electrochemical, magnetic, and mechanical means[7]. Nevertheless, the operating principles of these solid-state devices are fundamentally distinct from those of the human brain, which relies on intricate physicochemical processes within an electrolytic environment[8]. More essentially, the human brain employs different neurochemicals to regulate memory kinetics[7,9]. his emphasizes that neurochemicals play pivotal roles in memory and signifies that truly biomimetic memory should be neurochemically diversifiable.

Aqueous neuromorphic techniques - the innovation of devices that speak chemical language in electrolytes - are currently experiencing substantial growth in research[10-12], driven by their potential to streamline the interface between artificial and biological systems. Among them, nanofluidic memristors[13-18] and organic electrochemical transistors (OECTs)[19-28] have been particularly explored. In terms of memory behaviors, enhanced memory has been achieved through slow ion transport in nanofluidic memristors[14] and large migrating ions in OECTs[29,30]. Nevertheless, neurochemical memory diversification remains challenging. To explore the biochemical events that modulate conductance, we previously proposed an organic photoelectrochemical transistor (OPECT) that links the realms of photoelectrochemistry[31-34] and OECTs. As it can perceive light-biochemical signals through parallel transmission of ions and molecules in electrolytes, this nascent technique has rapidly stood out as a promising approach to aqueous neuromorphic exploration[35-41].

By neurochemical mediation, reward-induced memory serves as a crucial basis for reward circuitry supporting advanced learning and decision-making in the human brain[42-44]. Inspired by such neurochemical reward mechanisms, reinforcement learning (RL) has emerged as a powerful machine learning paradigm. RL algorithms use reward-driven feedback to optimize decision-making strategies, mirroring the adaptive learning process of the brain[45-54]. To implement RL neural networks, synaptic weights are commonly adjusted through correlations between timing and reward signals[52]. In this process, diversified memory is indispensable, as it supports reward-induced updating and maintenance of device conductance[48-50]. For instance, Sarwat *et al*. used the combined effects of light and electrical stimuli to tune memory for RL in a solid-state chalcogenide optomemristor[46]. Despite this progress, aqueous implementation of RL, especially that mediated by real neurochemicals, remains unexplored. Here, we report neurochemical memory diversification on OPECTs toward RL in aqueous media.

EXPERIMENTAL

Materials

Polyvinylpyrrolidone (PVP), $CdCl_2 \cdot xH_2O$, and $Na_2S \cdot 9H_2O$ were obtained from Aladdin Biochemical Technology Co., Ltd. (Shanghai, China). The compound 2-methylimidazole (2-MI) was purchased from Sigma-Aldrich (St. Louis, MO, USA). $Zn(NO_3)_2 \cdot 6H_2O$ was purchased from Xilong Scientific Co., Ltd. (Shantou, China). A poly(3,4-ethylenedioxythiophene):poly(styrenesulfonate) (PEDOT:PSS) dispersion (Clevios PH1000) was obtained from Heraeus Ltd. (Hanau, Germany).

Fabrication of Cd^{2+}/ZnO electrode

PVP (0.2 g) was dissolved in 40 mL of deionized water under magnetic stirring. Subsequently, 4 mL of an aqueous solution containing 0.6568 g of 2-MI was introduced into the PVP solution under continuous stirring, followed by the dropwise addition of 4 mL of an aqueous solution of $Zn(NO_3)_2 \cdot 6H_2O$ (0.238 g). After complete dissolution, the mixture was kept undisturbed for 24 h. The resulting precipitate was washed three

times with deionized water and ethanol, respectively, and dried at 60 °C to yield zeolitic imidazolate framework-L (ZIF-L). The obtained ZIF-L was then calcined in a muffle furnace: first heated to 350 °C at 2 °C·min^{-1} and maintained for 60 min, then increased to 450 °C at 1 °C·min^{-1} and maintained for 30 min, affording ZIF-L-derived ZnO. Next, ZnO was dispersed in deionized water to form a suspension (2 mg·mL^{-1}), which was drop-cast onto indium tin oxide (ITO) substrates and dried at 60 °C. The ZnO/ITO electrodes were then immersed in a 10 mM $CdCl_2 \cdot xH_2O$ aqueous solution for 30 min and dried at 37 °C for 30 min to obtain the Cd^{2+}/ZnO electrode.

H_2S and H_2O_2 treatment

In a 5 mL centrifuge tube, 2 mL of a $Na_2S \cdot 9H_2O$ solution at a specified concentration was prepared, and the Cd^{2+}/ZnO electrode obtained was immersed in it for 1 h. The electrode was then rinsed with deionized water to remove residual ions, followed by drying at 37 °C for 30 min to obtain the CdS/ZnO electrode. On the other hand, to etch the CdS, a mixed solution of horseradish peroxidase (HRP, 1 mg/mL) and H_2O_2 at a specified concentration was prepared and thoroughly mixed. A volume of 25 μL of this solution was dropped onto the CdS/ZnO electrode, followed by incubation at room temperature for 15 min, rinsing with water, and drying at 37 °C for 30 min.

Fabrication of polymeric channel[38]

First, a 10 nm Cr layer and a 100 nm Au layer were deposited onto a glass substrate covered by a shadow mask. The length and width of the channel were 6 mm and 0.2 mm, respectively. Subsequently, 0.1 mL of PEDOT:PSS dispersion containing 5% (v/v) dimethyl sulfoxide was dropped onto the substrate, spin-coated at 4,000 rpm for 30 s, and annealed at 180 °C for 1 h.

Device characterization

The electrical signals were recorded using a photoelectrochemical/organic transistor detector (Nandaguang, Nanjing, China) in the phosphate-buffered saline (PBS) electrolyte. The channel voltage was set to 0.1 V during testing.

Design of the RL algorithm

To implement RL for the navigation task, we used a simple weight-update rule based on the device's response to neurochemical inputs. The postsynaptic current response (ΔPSC) was modeled as a function of pulse number, derived from experimental measurements under repeated light pulses. The long-term (ltm) and short-term (stm) components of ΔPSC were expressed as:

$$ltm = -245.09 + 131.58 \times \ln(current\_ep + 6.13) \quad (1)$$

$$stm = -54.57 + 12.27 \times \ln(current\_ep + 83.32) \quad (2)$$

where current_ep is the postsynaptic current measured at the ep-th light pulse, and the constants are fitting parameters obtained from experimental data. These functions describe how the synaptic conductance evolves with the number of presynaptic spikes (simulated by light pulses) under the influence of H_2S (reward) or H_2O_2 (clearance).

The function was then used for training in MATLAB (MATrix LABoratory). Whenever the rodent reached the endpoint, the reward signal (H_2S) was applied, and the synaptic weights corresponding to the taken path were updated according to the fitted reward-response curve. Conversely, when the reward was cleared (H_2O_2), the weights were updated using the clearance-response curve. This approach allowed the synaptic connections to be strengthened for rewarded paths and weakened for non-rewarded or erroneous ones, enabling the network to progressively learn the optimal route.

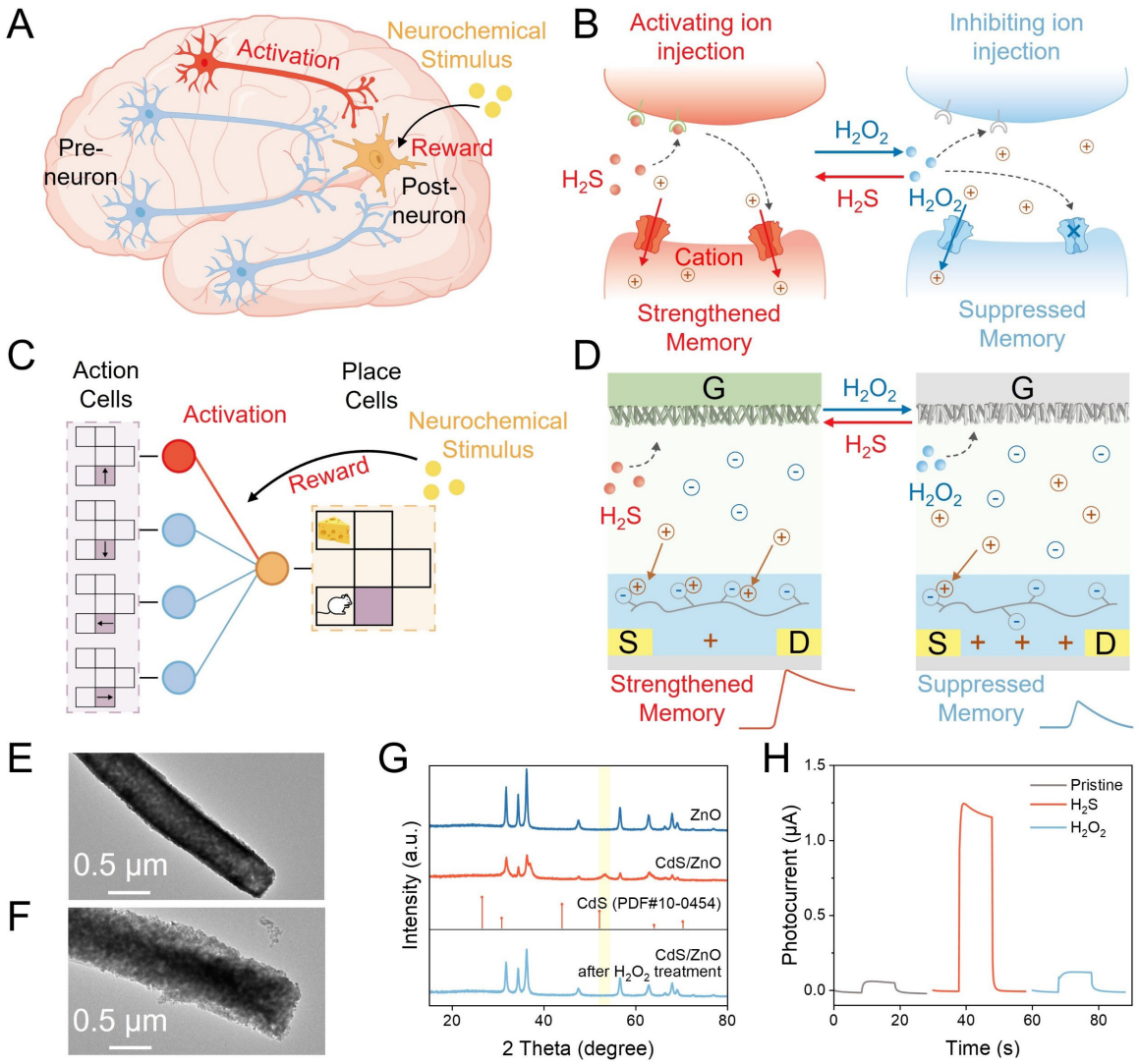

Figure 1. (A) Schematic illustration of reward learning in the human brain; (B) Schematic illustration of the biological strengthened memory and suppressed memory at the synaptic level; (C) Schematic illustration of the RL neural network diagram for navigation; (D) Schematic of the biological memory diversification of the device. TEM images of (E) ZnO and (F) CdS/ZnO; (G) XRD spectra of ZnO (blue curve), CdS/ZnO (red curve), and CdS/ZnO after H_2O_2 treatment (light blue curve); (H) Photocurrent responses of pristine electrode, H_2S-treated electrode, and H_2O_2-treated electrode. PDF: Powder Diffraction Powder; RL: reinforcement learning; XRD: X-ray diffraction; TEM: transmission electron microscopy.

RESULTS AND DISCUSSION

Design of theneurochemical-mediated RL

Figure 1A demonstrates the typical mechanism of reward-induced memory in the human brain. Specifically, in neural circuits, neurochemical stimuli act as reward signals that modulate synaptic plasticity in brain regions governing reward processing, thereby strengthening functional connections between specific neural pathways, underlying the induction of strengthened memory at these synapses[55]. This activity-dependent enhancement of neuronal communication enables the brain to encode reward-associated experiences, establishing a biological basis for how neurochemical inputs facilitate the learning and memory consolidation of rewarding behaviors. Down to the synaptic level, as shown in Figure 1B, such diversified memory dynamics are achieved by specific neurochemicals. Typically, the hydrogen sulfide (H_2S), as a well-known neurochemical, can lead to the inward flow of ions to induce strengthened memory[56]. On the other hand, reactive oxygen species (ROS), e.g., hydrogen peroxide (H_2O_2), can inhibit H_2S activity and thus reduce ion influx, thereby suppressing memory[57].

Taking this inspiration, an artificial neural network with RL was designed for a navigation application. As shown in Figure 1C, it consisted of presynaptic neurons encoding movement directions and postsynaptic neurons encoding positions, linked by artificial synapses. Analogous to that in the human brain, a real neurochemical stimulus was introduced as a reward signal to tune memory and thus update synaptic weights. Specifically, as shown in Figure 1D and Supplementary Figure 1, an OPECT synapse with memory diversification was developed, in which the PEDOT:PSS channel was modulated by a Cd^{2+}/ZnO photogate in aqueous media. The addition of H_2S as the reward, would enhance photo-induced voltage, driving more cations into the channel and thus strengthening memory. By contrast, the addition of H_2O_2 would reduce the clearance of CdS, leading to lower photo-induced voltage, inhibiting cation injection into the channel, and thus suppressing memory. Such a neurochemically dependent memory can be implemented to adjust the conductivity for updating synaptic weights in the RL neural network.

The successful fabrication of the device was characterized as shown in Supplementary Figures 2-5. As presented in Figure 1E and F, the transmission electron microscopy (TEM) images revealed that after the treatment of H_2S, many particles were generated on the surface of ZnO, which were confirmed as CdS by corresponding energy-dispersive spectroscopy (EDS) mapping, as shown in Supplementary Figure 6. The X-ray photoelectron spectroscopy (XPS) spectra in Supplementary Figure 7 also validated the formation of CdS. In addition, as shown in Figure 1G, the X-ray diffraction (XRD) spectra exhibited an extra characteristic peak of CdS after the treatment of H_2S, which disappeared after H_2O_2 treatment, indicating the reversible generation and clearance of CdS. The corresponding photoelectrochemical characteristics were further studied using a conventional three-electrode system. As shown in Figure 1H, the pristine Cd^{2+}/ZnO photogate exhibited a photocurrent of *ca.* 0.06 μA, while the treatment of H_2S caused a substantially enhanced photocurrent of *ca.* 1.2 μA. After further H_2O_2 treatment, the photocurrent returned to *ca.* 0.12 μA. Such phenomena could be explained by the mechanism illustrated in Supplementary Figure 8, which is further supported by the light-absorption results shown in Supplementary Figure 9.

Neurochemical-mediated diversified memory

Figure 2A presents the ΔPSC of the OPECT device before and after the treatment of H_2S and H_2O_2. As shown, after H_2S treatment, the device exhibited substantially increased ΔPSC and slower return to the initial level. By contrast, after subsequent treatment with H_2O_2, the ΔPSC decreased with a faster decay, which, nevertheless, was still higher than that of the pristine photogate due to the residual CdS. To evaluate variation in memory behavior, the memory time (defined as the time required for the ΔPSC to decay to 1% of its peak value) was investigated by calculating the extrapolated horizontal of the decay curves. As shown in Figure 2B, compared to the 230 s memory time of the pristine device, the memory time after H_2S treatment exceeded 40,000 s, indicating the significantly enhanced memory behavior. Furthermore, a comparative analysis with other reported optoelectronic synaptic devices was performed, as summarized in Supplementary Table 1, which revealed that the memory performance of this device was markedly superior to that of previously reported systems. The treatment with H_2O_2 would result in a decreased memory time of *ca.* 300 s, indicating the adjustable memory behavior.

The mechanism of such a phenomenon could be attributed to altered electron-transfer dynamics. As shown in Figure 2C, the presence of H_2S resulted in the formation of CdS/ZnO Z-scheme heterojunction[58]. Upon light illumination, the photo-excited electrons on the conduction band (CB) of CdS would transfer to the valence band (VB) of ZnO, and the photo-excited electrons on the CB of ZnO would transfer to the substrate electrode, producing a photo-induced voltage. Under light illumination, the residual electrons on the CB of ZnO and holes on the VB of CdS were difficult to recombine due to the bending of energy bands, leading to slow decay of the photo-induced voltage and thus the generation of strengthened memory. On the other hand, the treatment of H_2O_2 would result in the clearance of CdS. Upon light illumination, the as-treated device could generate a much lower photo-induced voltage, leading to a decreased ΔPSC. Under light

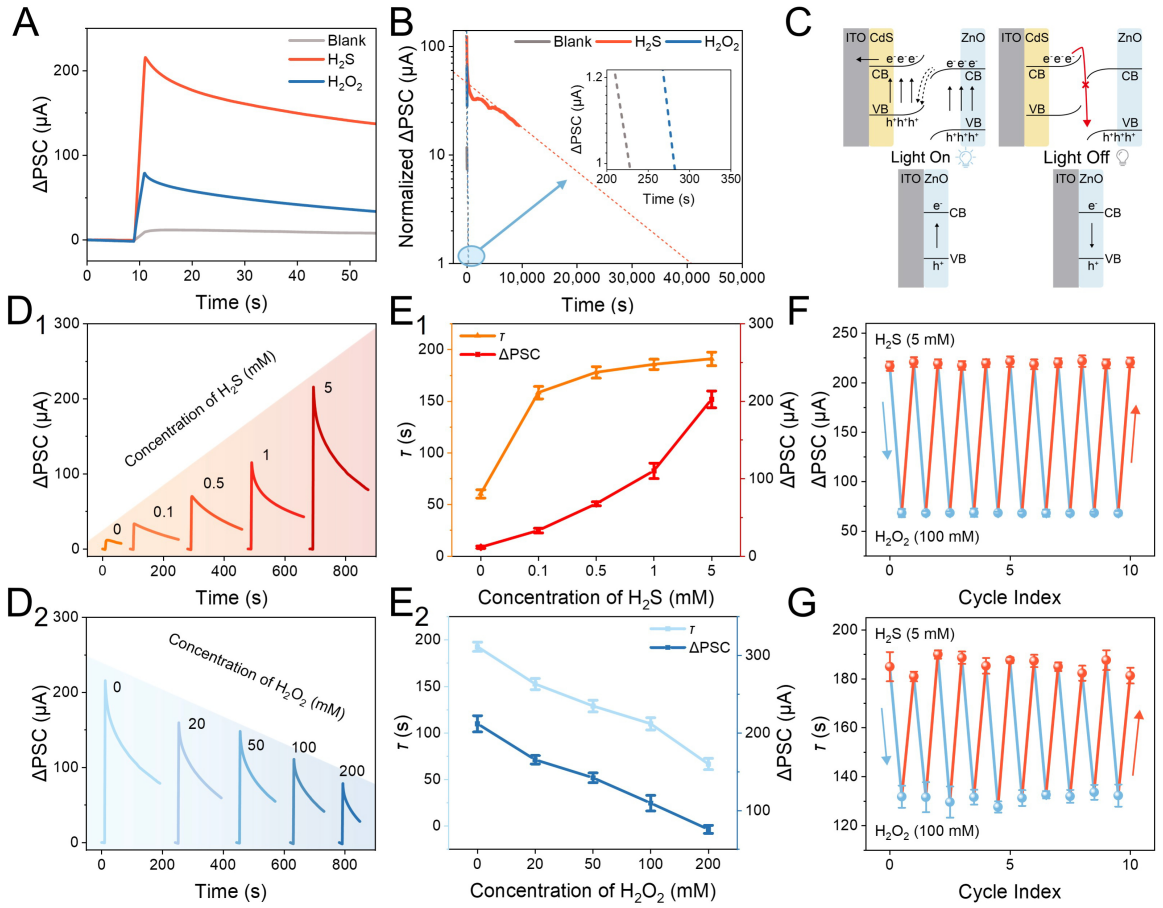

Figure 2. All light used was 2 s 15.17 mW·cm^{-2}. (A) ΔPSC responses and (B) the decay of the pristine device and that after the treatment of H_2S and subsequent H_2O_2; (C) Mechanism of diversified memory dynamics from the perspective of electron transfer. ΔPSC responses after the treatment of (D_1) H_2S and (D_2) H_2O_2 with different concentrations; Variations of τ and ΔPSC with the increased (E_1) H_2S and (E_2) H_2O_2 concentrations; Recyclability of (F) ΔPSC and (G) τ upon alternating H_2S and H_2O_2 treatments. ΔPSC: Postsynaptic current response; H_2S: hydrogen sulfide; H_2O_2: hydrogen peroxide; ITO: indium tin oxide; CB: conduction band; VB: valence band.

illumination, rapid electron-hole recombination led to a faster decay of the photo-induced voltage and thus to suppressed memory. This phenomenon was further corroborated by the open-circuit potential (OCP) and electrical pulse response results, as shown in Supplementary Figures 10 and 11.

The relationship between neurochemical concentrations and memory behaviors was then studied. As shown in Figure 2D$_1$, with increased H_2S concentrations, the device exhibited gradually increased ΔPSC due to the increased production of CdS. Conversely, as shown in Figure 2D$_2$, increasing H_2O_2 concentrations would result in a decreased ΔPSC, due to greater heterojunction destruction. As shown in Figure 2E$_1$ and E$_2$, the as-calculated characteristic decay time τ (defined as the time required for current to decay from the peak to 1/e of the peak value) increased with increasing H_2S concentration and decreased with increasing H_2O_2 concentration, indicating improved and suppressed memory, respectively. Such results were highly analogous to the H_2S and H_2O_2-mediated memory and forgetting in the human brain[56,57]. Moreover, as shown in Figure 2F and G, both the ΔPSC and τ values exhibited reversible and reproducible changes upon three cycles of H_2S and H_2O_2 treatments, confirming the recyclable memory behavior. In addition, the effects of varying ionic strength, pH, oxygen concentration, and different interfering species on device performance were systematically investigated, as shown in Supplementary Figure 12, further demonstrating the specificity and stability of the device.

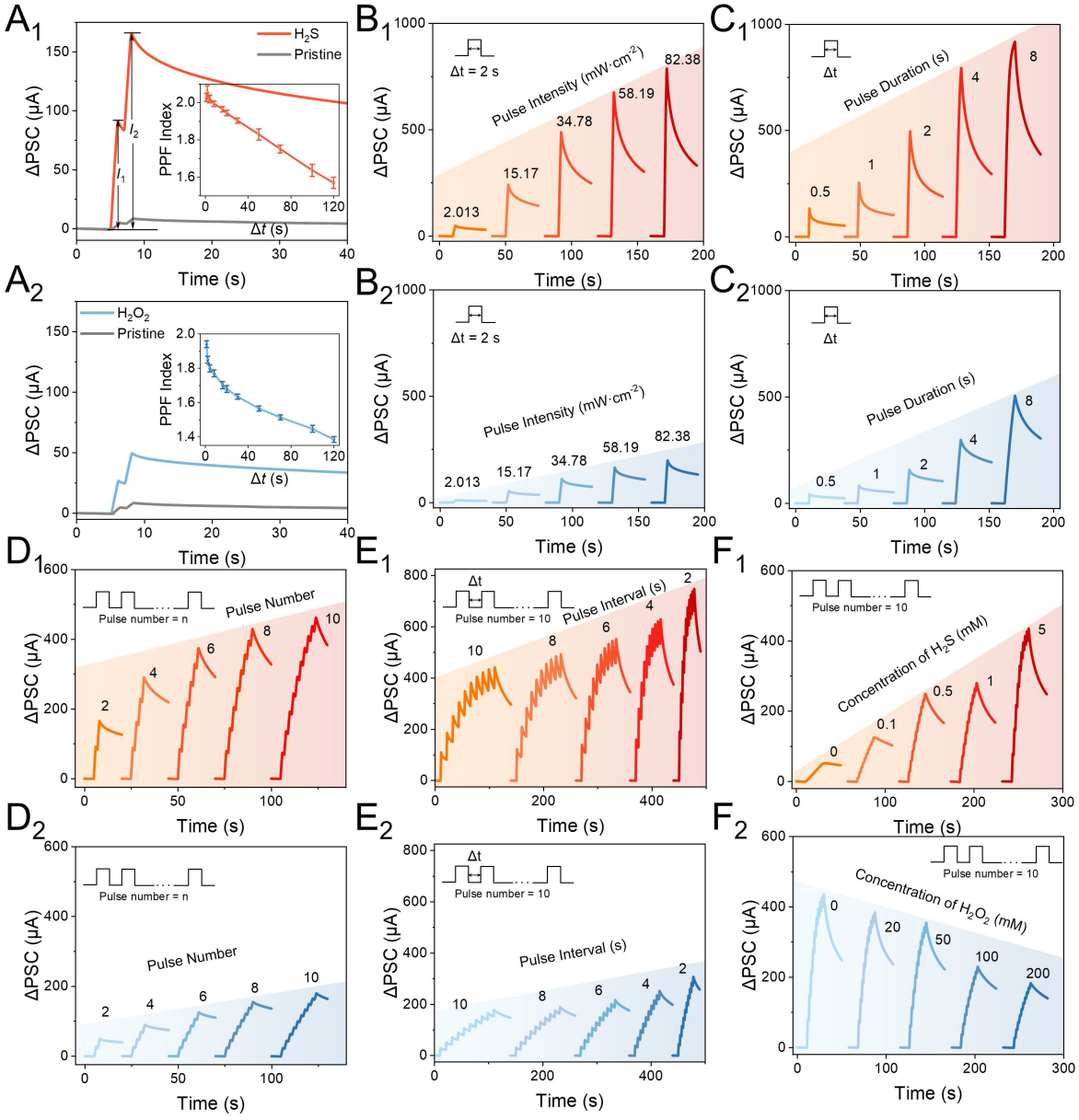

Figure 3. PPF behaviors of (A_1) the pristine devices, and those after the treatment of H_2S, and (A_2) the pristine devices, and those after the treatment of H_2O_2; The inset shows the PPF indices for different pulse intervals (1 s, 15.17 mW·cm^{-2} light pulses). SIDP emulation of the device after the treatment of (B_1) H_2S and (B_2) H_2O_2 with light intensities ranging from 2.013 mW·cm^{-2} to 82.38 mW·cm^{-2} (1 s light pulses); SDDP emulation of the device after treatment of (C_1) H_2S and (C_2) H_2O_2 with pulse durations ranging from 0.5 s to 8 s (15.17 mW·cm^{-2} light pulses); SNDP emulation of the device after treatment of (D_1) H_2S and (D_2) H_2O_2 with 2 to 10 pulses (15.17 mW·cm^{-2} light pulses); SRDP emulation of the device after treatment of (E_1) H_2S and (E_2) H_2O_2 with light pulse intervals ranging from 10 s to 2 s (1 s, 15.17 mW·cm^{-2} light pulses); (F_1) H_2S-mediated synaptic plasticity; (F_2) H_2O_2-mediated synaptic plasticity (1 s, 15.17 mW·cm^{-2} light pulses). ΔPSC: Postsynaptic current response; PPF: paired-pulse facilitation; H_2S: hydrogen sulfide; H_2O_2: hydrogen peroxide; SIDP: spike-intensity-dependent plasticity; SDDP: spike-duration-dependent plasticity; SNDP: spike-number-dependent plasticity; SRDP: spike-rate-dependent plasticity.

Neurochemical-mediated synaptic plasticity

In the human brain, synaptic plasticity represents a fundamental function underlying memory and learning[59]. In the reward circuitry, synaptic plasticity is mediated by neurochemical reward signals, inducing widespread alterations in the neural network[60]. Here, neurochemical-mediated short-term plasticity was initially emulated by applying two light pulses with the treatments H_2S and H_2O_2, respectively. As shown in Figure 3A_1 and A_2, the ΔPSC exhibited typical paired-pulse facilitation (PPF) behavior. Notably, compared to that of the pristine device, the addition of H_2S resulted in both enhanced ΔPSC value, improved PPF index (I_2/I_1), and slower decay of the PPF index with increased interval (Δt), emulating the reward-mediated

strengthened memory, which was further inhibited by the addition of H_2O_2.

Spike-dependent plasticity represents another significant plasticity demonstrating the relationship between synaptic weight and the characteristics of spikes, which was also studied by biochemical reward signals. As shown in Figure 3B_1 and B_2, higher light intensity caused ΔPSC to rise progressively and exhibit slower retention to the initial level, mimicking spike-intensity-dependent plasticity (SIDP). As shown in Figure 3C_1 and C_2, longer pulse duration also resulted in larger ΔPSC and slower retention, mimicking spike-duration-dependent plasticity (SDDP). Moreover, as shown in Figure 3D and E, increasing the pulse number and shortening the pulse interval led to enhanced ΔPSC, emulating spike-number-dependent plasticity (SNDP) and spike-rate-dependent plasticity (SRDP), respectively. Significantly, with the addition of H_2S, the ΔPSC exhibited enhanced variation with changed pulse characteristics and the retention time substantially improved as compared to that of H_2O_2, which was highly analogous to the reward-mediated plasticity in biology[54,55]. Significantly, the relationship between the concentrations of neurochemicals and synaptic plasticity was studied. As shown in Figure 3F_1 and F_2, increased H_2S concentration resulted in enhanced ΔPSC and memory, while increased H_2O_2 concentration led to suppressed ΔPSC and memory, which was analogous to that in biology.

Emulation of the RL

Navigation is a standard task to investigate the performance of RL and the corresponding hardware designs[46,61]. Principally, the feedback signals will induce strengthened/suppressed memory to strengthen/suppress the synaptic connection between specific locations and action neurons, resulting in the habitual action at the corresponding location. Here, we present an example game: a rodent trapped in a maze to search for cheese and avoid obstacles. Specifically, as shown in Figure 4A, the maze consisted of 6 positions (white blocks), including a starting point and an endpoint, and a surrounding circle of walls (black blocks). The rodent had 4 possible directions of motion at these positions. Therefore, a 5 × 4 neural network was constructed to determine the movement at each position, with the device conductance serving as synaptic weights, representing the probability of each direction. Light pulses were applied to emulate the presynaptic spikes that record the traversed paths. Each pulse triggered a photoresponse in the OPECT synapse, modulating channel conductance and hence the synaptic weight associated with that movement direction. As the rodent explored the maze, different paths generated different sequences of light pulses, corresponding to the activation of specific position-direction synapses, inducing variation of synaptic weights linking corresponding positions and directions. H_2S and H_2O_2 served as reward signals and reward clearance, respectively. The specific training process of RL was illustrated in Figure 4B. As shown, before training, the rodent engaged in random exploration of the maze. If it failed to reach the endpoint after 50 steps or collided with a wall, it was returned to the starting point. Once the rodent successfully reached the endpoint, the H_2S reward signal was applied, strengthening memory and updating the synaptic weights of the traversed paths. It was then returned to the starting point for the next training epoch, and H_2O_2 cleared the reward, recovering the suppressed memory. After reinforcement learning, the rodent was able to find the shortest path to the endpoint.

Such a process was then experimentally realized by H_2S- and H_2O_2-mediated memory. As shown in Figure 4C, the addition of H_2S resulted in a substantially enhanced Δconductance (red curve), while the addition of H_2O_2 caused a much-suppressed Δconductance with increased light pulse number (blue curve). Moreover, as shown in Supplementary Figure 13, the conductance window and the nonlinearity were measured, revealing that the H_2S-treated device was suitable for RL. As shown in Figure 4D, with the assistance of a reward, the rodent found the shortest path after four training trials and continued to choose it after 27 training trials. Repeated tests, shown in Supplementary Figure 14, all yielded similarly successful outcomes. As shown in Figure 4E, the synaptic weights corresponding to the shortest path (position 1 moves right, positions 2 and 3 move upward, and position 5 moves left) were substantially enhanced, indicating successful training. By

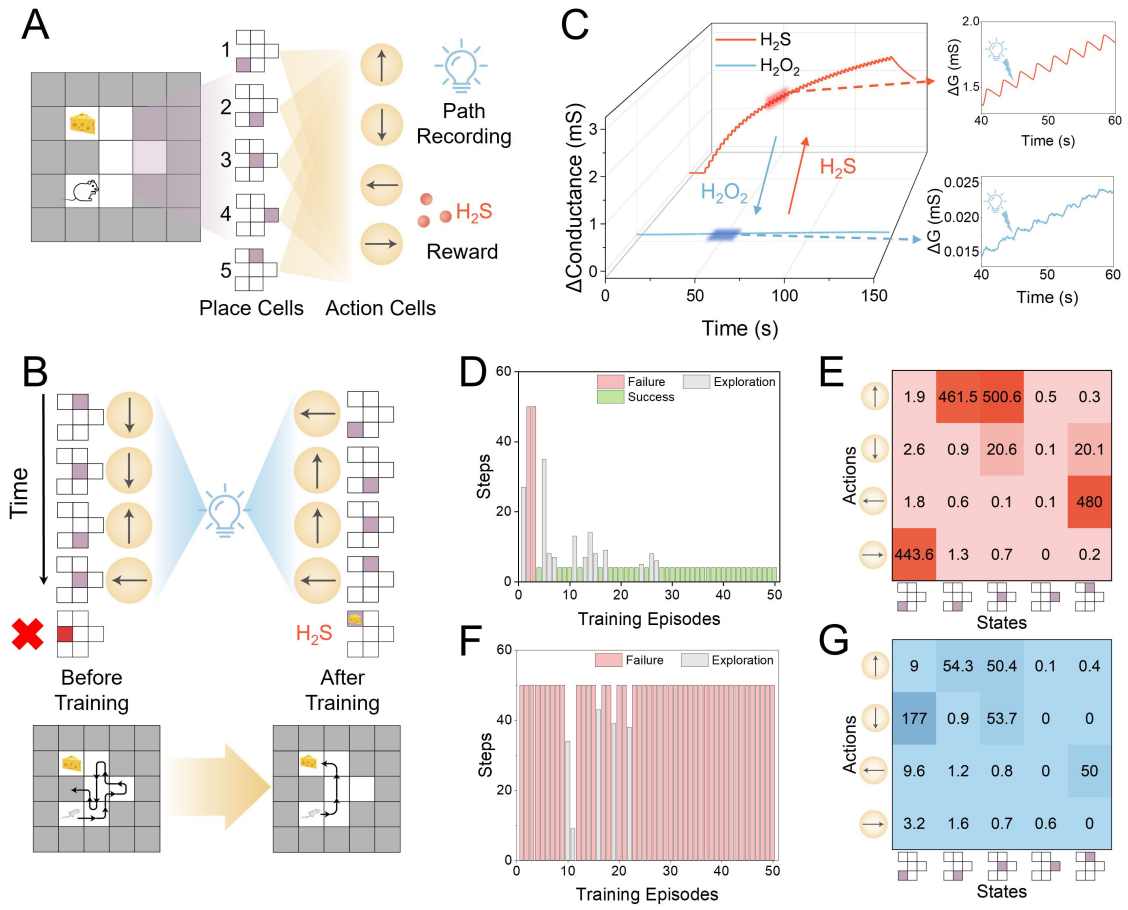

Figure 4. (A) Schematic of a rodent navigation task; (B) Training process of the navigation; (C) Device responses under 50 continuous light pulses after the treatment of H_2S (red curve) and H_2O_2 (blue curve) (2 s, 15.17 mW·cm^{-2} light pulses); (D) Exploration result with increased training epochs with the assistance of a reward; (E) Synaptic weights matrix after training with the assistance of a reward; (F) Exploration result with increased training epochs without the assistance of a reward; (G) Synaptic weights matrix after training without the assistance of a reward. H_2S: Hydrogen sulfide; H_2O_2: hydrogen peroxide; ΔG: ΔConductance.

contrast, as shown in Figure 4F, without the reward, the rodent reached the endpoint only five times, and the shortest path was not identified. As shown in Figure 4G, the synaptic weights corresponding to the wrong path (positions 1 and 3 move downward) were enhanced. These results indicate the capability of RL to improve training efficiency. If the reward function was replaced with a stochastic reward function, the training process, as shown in Supplementary Figure 15A, was dominated by maze exploration for the majority of trials. In addition, when the reward function was set to a constant value (e.g., 10), the rodent more frequently identified the shortest path, as shown in Supplementary Figure 15B. Moreover, we extended the proposed method to a larger 4 × 5 maze, as shown in Supplementary Figure 16, and the results demonstrated that the shortest path could still be successfully identified.

CONCLUSIONS

In conclusion, this work establishes a new paradigm for neurochemical memory diversification on OPECT towards liquid-phase RL, in which H_2S and H_2O_2 serve as reward and clearance signals to reversibly regulate memory states. Beyond reproducing fundamental synaptic plasticity such as PPF and spike-dependent plasticity, it enables dynamic modulation of device conductance and, consequently, diversified memory behaviors. Importantly, by implementing these neurochemical-regulated functions in a navigation task, we verify the capability of neurochemical memory diversification to support efficient RL in aqueous media. To the best of our knowledge, this study demonstrates the first neurochemical memory diversification in an

organic transistor operating in liquid, and we anticipate that this approach will inspire higher-level biological memory analogs for neuromorphic applications.

DECLARATIONS

Authors' contributions

Made substantial contributions to conception and design of the study and performed data analysis and interpretation: Lou, H.; Yuan, C.
Performed data acquisition: Zhu, Y. C.; Chen, F. Z.; Jia, H. M.
Provided administrative, technical, and material support: Xu, J. J.; Zhao, W. W.
Lou, H.; Yuan, C. contributed equally to this work.

Availability of data and materials

The raw data supporting the conclusions of this article will be made available by the authors upon request.

Financial support and sponsorship

This work was supported by the National Natural Science Foundation of China (22174063 and 22374066) and the Excellent Research Program of Nanjing University (ZYJH004).

Conflicts of interest

Zhao, W. W. is an Editorial Board Member of the journal *Iontronics* but is not involved in any steps of the editorial process, notably including reviewer selection, manuscript handling, or decision-making, while the other authors declared that there have no conflicts of interest.

Ethical approval and consent to participate

Not applicable.

Consent for publication

Not applicable.

Supplementary Materials

Supplementary Materials

REFERENCES

1. Dudai, Y.; Karni, A.; Born, J. The consolidation and transformation of memory. *Neuron* **2015**, *88*, 20-32. DOI PubMed
2. McGaugh, J. L. Memory - a century of consolidation. *Science* **2000**, *287*, 248-51. DOI PubMed
3. Josselyn, S. A.; Tonegawa, S. Memory engrams: recalling the past and imagining the future. *Science* **2020**, *367*. DOI PubMed PMC
4. Zidan, M. A.; Strachan, J. P.; Lu, W. D. The future of electronics based on memristive systems. *Nat. Electron.* **2018**, *1*, 22-9. DOI
5. Li, C.; Belkin, D.; Li, Y.; et al. Efficient and self-adaptive in-situ learning in multilayer memristor neural networks. *Nat. Commun.* **2018**, *9*, 2385. DOI PubMed PMC
6. Zhong, Y.; Tang, J.; Li, X.; Gao, B.; Qian, H.; Wu, H. Dynamic memristor-based reservoir computing for high-efficiency temporal signal processing. *Nat. Commun.* **2021**, *12*, 408. DOI PubMed PMC
7. Chen, Y.; Han, B.; Gobbi, M.; Hou, L.; Samorì, P. Responsive molecules for organic neuromorphic devices: harnessing memory diversification. *Adv. Mater.* **2025**, *37*, e2418281. DOI PubMed PMC
8. Titley, H. K.; Brunel, N.; Hansel, C. Toward a neurocentric view of learning. *Neuron* **2017**, *95*, 19-32. DOI PubMed PMC
9. Magistretti, P. J.; Allaman, I. Lactate in the brain: from metabolic end-product to signalling molecule. *Nat. Rev. Neurosci.* **2018**, *19*, 235-49. DOI PubMed
10. He, K.; Wang, C.; He, Y.; Su, J.; Chen, X. Artificial neuron devices. *Chem. Rev.* **2023**, *123*, 13796-865. DOI PubMed
11. Harikesh, P. C.; Tu, D.; Fabiano, S. Organic electrochemical neurons for neuromorphic perception. *Nat. Electron.* **2024**, *7*, 525-36. DOI
12. Sung, M. J.; Kim, K. N.; Kim, C.; et al. Organic artificial nerves: neuromorphic robotics and bioelectronics. *Chem. Rev.* **2025**, *125*, 2625-64. DOI PubMed

13. Xiong, T.; Li, C.; He, X.; et al. Neuromorphic functions with a polyelectrolyte-confined fluidic memristor. *Science* **2023**, *379*, 156-61. DOI PubMed
14. Robin, P.; Emmerich, T.; Ismail, A.; et al. Long-term memory and synapse-like dynamics in two-dimensional nanofluidic channels. *Science* **2023**, *379*, 161-7. DOI PubMed
15. Emmerich, T.; Teng, Y.; Ronceray, N.; et al. Nanofluidic logic with mechano-ionic memristive switches. *Nat. Electron.* **2024**, *7*, 271-8. DOI PubMed PMC
16. Xiao, Y.; Sun, W.; Gao, C.; et al. Neural functions enabled by a polarity-switchable nanofluidic memristor. *Nano. Lett.* **2024**, *24*, 12515-21. DOI PubMed
17. Song, R.; Wang, P.; Zeng, H.; et al. Nanofluidic memristive transition and synaptic emulation in atomically thin pores. *Nano. Lett.* **2025**, *25*, 5646-55. DOI
18. Wang, Y.; Jian, B.; Ling, Y.; et al. Bioinspired nanofluidic circuits with integrating excitatory and inhibitory synapses. *Nano. Lett.* **2025**, *25*, 2298-306. DOI PubMed
19. Chen, X.; Marks, A.; Paulsen, B. D.; et al. n-type rigid semiconducting polymers bearing oligo(ethylene glycol) side chains for high-performance organic electrochemical transistors. *Angew. Chem. Int. Ed. Engl.* **2021**, *60*, 9368-73. DOI PubMed
20. Harikesh, P. C.; Yang, C. Y.; Wu, H. Y.; et al. Ion-tunable antiambipolarity in mixed ion-electron conducting polymers enables biorealistic organic electrochemical neurons. *Nat. Mater.* **2023**, *22*, 242-8. DOI PubMed PMC
21. Huang, W.; Chen, J.; Yao, Y.; et al. Vertical organic electrochemical transistors for complementary circuits. *Nature* **2023**, *613*, 496-502. DOI PubMed PMC
22. Song, J.; Liu, H.; Zhao, Z.; et al. 2D metal-organic frameworks for ultraflexible electrochemical transistors with high transconductance and fast response speeds. *Sci. Adv.* **2023**, *9*, eadd9627. DOI PubMed PMC
23. Cucchi, M.; Parker, D.; Stavrinidou, E.; Gkoupidenis, P.; Kleemann, H. In liquido computation with electrochemical transistors and mixed conductors for intelligent bioelectronics. *Adv. Mater.* **2023**, *35*, e2209516. DOI PubMed
24. Ding, B.; Kim, G.; Kim, Y.; et al. Influence of backbone curvature on the organic electrochemical transistor performance of glycolated donor-acceptor conjugated polymers. *Angew. Chem. Int. Ed. Engl.* **2021**, *60*, 19679-84. DOI PubMed PMC
25. Laswick, Z.; Wu, X.; Surendran, A.; et al. Tunable anti-ambipolar vertical bilayer organic electrochemical transistor enable neuromorphic retinal pathway. *Nat. Commun.* **2024**, *15*, 6309. DOI PubMed PMC
26. Lobosco, A.; Lubrano, C.; Rana, D.; et al. Enzyme-mediated organic neurohybrid synapses. *Adv. Mater.* **2024**, *36*, e2409614. DOI PubMed PMC
27. Matrone, G. M.; van Doremaele, E. R. W.; Surendran, A.; et al. A modular organic neuromorphic spiking circuit for retina-inspired sensory coding and neurotransmitter-mediated neural pathways. *Nat. Commun.* **2024**, *15*, 2868. DOI PubMed PMC
28. Wang, S.; Wang, Y.; Cai, X.; et al. A high-frequency artificial nerve based on homogeneously integrated organic electrochemical transistors. *Nat. Electron.* **2025**, *8*, 254-66. DOI
29. Liu, X.; Dai, S.; Zhao, W.; et al. All-photolithography fabrication of ion-gated flexible organic transistor array for multimode neuromorphic computing. *Adv. Mater.* **2024**, *36*, e2312473. DOI PubMed
30. Liu, R.; He, Y.; Zhu, X.; et al. Hardware-feasible and efficient n-type organic neuromorphic signal recognition via reservoir computing. *Adv. Mater.* **2025**, *37*, e2409258. DOI PubMed
31. Wang, C.; Wang, Y.; Kirlikovali, K. O.; et al. Ultrafine silver nanoparticle encapsulated porous molecular traps for discriminative photoelectrochemical detection of mustard gas simulants by synergistic size-exclusion and site-specific recognition. *Adv. Mater.* **2022**, *34*, e2202287. DOI PubMed
32. Huang, H.; Li, Z.; Li, Z.; et al. Photoelectrochemical lithium extraction. *Nano. Energy.* **2023**, *115*, 108683. DOI
33. Huang, C.; Xiong, P.; Lai, X.; Xu, H. Photoelectrochemical asymmetric catalysis. *Nat. Catal.* **2024**, *7*, 1250-4. DOI
34. Gu, S.; Xu, D.; Huang, J.; Zhou, X.; Liu, Y.; Zhang, Z. Photoelectrochemical biosensor with single atom sites for norepinephrine sensing and brain region synergy in epilepsy. *Nat. Commun.* **2025**, *16*, 4765. DOI PubMed PMC
35. Corrado, F.; Bruno, U.; Prato, M.; et al. Azobenzene-based optoelectronic transistors for neurohybrid building blocks. *Nat. Commun.* **2023**, *14*, 6760. DOI PubMed PMC
36. Druet, V.; Ohayon, D.; Petoukhoff, C. E.; et al. A single n-type semiconducting polymer-based photo-electrochemical transistor. *Nat. Commun.* **2023**, *14*, 5481. DOI PubMed PMC
37. Li, Z.; Chen, M. H.; Wu, Q. Q.; et al. A metal-organic framework neuron. *Natl. Sci. Rev.* **2025**, *12*, nwaf213. DOI PubMed PMC
38. Yuan, C.; Xu, K. X.; Huang, Y. T.; Xu, J. J.; Zhao, W. W. An aquatic autonomic nervous system. *Adv. Mater.* **2024**, *36*, e2407654. DOI PubMed
39. Gao, C.; Liu, D.; Xu, C.; et al. Feedforward photoadaptive organic neuromorphic transistor with mixed-weight plasticity for augmenting perception. *Adv. Funct. Mater.* **2024**, *34*, 2313217. DOI

40. Wu, J.; Wang, X.; Tang, X.; et al. Low-power and multimodal organic photoelectric synaptic transistors modulated by photoisomerization for UV damage perception and artificial visual recognition. *Adv. Funct. Mater.* **2025**, *35*, 2420073. DOI
41. Wang, Y.; Shan, W.; Li, H.; et al. An optoelectrochemical synapse based on a single-component n-type mixed conductor. *Nat. Commun.* **2025**, *16*, 1615. DOI PubMed PMC
42. Braun, E. K.; Wimmer, G. E.; Shohamy, D. Retroactive and graded prioritization of memory by reward. *Nat. Commun.* **2018**, *9*, 4886. DOI PubMed PMC
43. Pedamonti, D.; Mohinta, S.; Dimitrov, M. V.; Malagon-Vina, H.; Ciocchi, S.; Costa, R. P. Hippocampus supports multi-task reinforcement learning under partial observability. *Nat. Commun.* **2025**, *16*, 9619. DOI PubMed PMC
44. Golden, C. E. M.; Martin, A. C.; Kaur, D.; et al. Estrogen modulates reward prediction errors and reinforcement learning. *Nat. Neurosci.* **2025**, *28*, 2502-14. DOI PubMed PMC
45. Mnih, V.; Kavukcuoglu, K.; Silver, D.; et al. Human-level control through deep reinforcement learning. *Nature* **2015**, *518*, 529-33. DOI PubMed
46. Sarwat, S. G.; Moraitis, T.; Wright, C. D.; Bhaskaran, H. Chalcogenide optomemristors for multi-factor neuromorphic computation. *Nat. Commun.* **2022**, *13*, 2247. DOI PubMed PMC
47. Romero Pinto, S.; Uchida, N. Tonic dopamine and biases in value learning linked through a biologically inspired reinforcement learning model. *Nat. Commun.* **2025**, *16*, 7529. DOI PubMed PMC
48. Weilenmann, C.; Ziogas, A. N.; Zellweger, T.; et al. Single neuromorphic memristor closely emulates multiple synaptic mechanisms for energy efficient neural networks. *Nat. Commun.* **2024**, *15*, 6898. DOI PubMed PMC
49. Wang, Z.; Li, C.; Song, W.; et al. Reinforcement learning with analogue memristor arrays. *Nat. Electron.* **2019**, *2*, 115-24. DOI
50. Xia, Q.; Yang, J. J. Memristive crossbar arrays for brain-inspired computing. *Nat. Mater.* **2019**, *18*, 309-23. DOI PubMed
51. Tomov, M. S.; Schulz, E.; Gershman, S. J. Multi-task reinforcement learning in humans. *Nat. Hum. Behav.* **2021**, *5*, 764-73. DOI PubMed
52. Zhou, Y.; Wang, Y.; Zhuge, F.; et al. A reconfigurable two-WSe_2 -transistor synaptic cell for reinforcement learning. *Adv. Mater.* **2022**, *34*, e2107754. DOI PubMed
53. Li, Z.; Myers, S. K.; Xiao, J.; et al. Neuromorphic ionic computing in droplet interface synapses. *Sci. Adv.* **2025**, *11*, eadv6603. DOI PubMed PMC
54. Im, J.; Kim, J.; Ko, J.; et al. Hybrid functional 3D artificial synapses for convolution and reinforcement learning. *Sci. Adv.* **2025**, *11*, eadw7498. DOI PubMed
55. Kunz, L.; Staresina, B. P.; Reinacher, P. C.; et al. Ripple-locked coactivity of stimulus-specific neurons and human associative memory. *Nat. Neurosci.* **2024**, *27*, 587-99. DOI PubMed PMC
56. Wang, R. Physiological implications of hydrogen sulfide: a whiff exploration that blossomed. *Physiol. Rev.* **2012**, *92*, 791-896. DOI PubMed PMC
57. Butterfield, D. A.; Halliwell, B. Oxidative stress, dysfunctional glucose metabolism and Alzheimer disease. *Nat. Rev. Neurosci.* **2019**, *20*, 148-60. DOI PubMed PMC
58. Wang, S.; Zhu, B.; Liu, M.; Zhang, L.; Yu, J.; Zhou, M. Direct Z-scheme ZnO/CdS hierarchical photocatalyst for enhanced photocatalytic H_2-production activity. *Appl. Catal. B:. Environ.* **2019**, *243*, 19-26. DOI
59. Kandel, E. R. The molecular biology of memory storage: a dialogue between genes and synapses. *Science* **2001**, *294*, 1030-8. DOI PubMed
60. Mills, F.; Globa, A. K.; Liu, S.; et al. Cadherins mediate cocaine-induced synaptic plasticity and behavioral conditioning. *Nat. Neurosci.* **2017**, *20*, 540-9. DOI PubMed PMC
61. Olin-Ammentorp, W.; Sokolov, Y.; Bazhenov, M. A dual-memory architecture for reinforcement learning on neuromorphic platforms. *Neuromorph. Comput. Eng.* **2021**, *1*, 024003. DOI